Characterising mass-resolved mixing state of Black Carbon in Beijing using a morphology-independent measurement method

Chenjie Yu[1], Dantong Liu[2,1], Kurtis Broda[3], Rutambhara Joshi[1], Jason Olfert[3], Yele Sun[4], Pingqing Fu[4,6], Hugh Coe[1], James D. Allan[1,5]

[1]School of Earth and Environmental Science, University of Manchester, Manchester, M13 9PL, UK
[2]Department of Atmospheric Sciences, School of Earth Sciences, Zhejiang University, Zhejiang, 310027, China
[3]Department of Mechanical Engineering, University of Alberta, Alberta, T6G 2R3, Canada
[4]Institute of Atmospheric Physics, Chinese Academy of Sciences, Beijing, 100029, China
[5]National Centre for Atmospheric Sciences, University of Manchester, Manchester, M13 9PL, UK
[6]Now at Institute of Surface-Earth System Science, Tianjin University, Tianjin, 300072, China

Correspondence to: Dantong Liu (dantongliu@zju.edu.cn), James Allan (james.allan@manchester.ac.uk)

Abstract. Refractory Black Carbon (rBC) in the atmosphere is known for its significant impacts on climate. The relationship between the microphysical and optical properties of rBC remains poorly understood and is influenced by its size and mixing state. Mixing state also influences its cloud scavenging potential and thus atmospheric lifetime. This study presents a coupling of a centrifugal particle mass analyser (CPMA) and a single particle soot photometer (SP2) for the morphology-independent quantification of the mixing state of rBC-containing particles, used in the urban site of Beijing as part of the Air Pollution and Human Health-Beijing (APHH-Beijing) project during winter (10th Nov – 10th Dec, 2016) and summer (18th May – 25th June, 2017). This represents a highly dynamic polluted environment with a wide variety of conditions that could be considered representative of megacity area sources in Asia. An inversion method (used for the first time on atmospheric aerosols) is applied to the measurements to present two-variable distributions of both rBC mass and total mass of rBC-containing particles and calculate the mass-resolved mixing state of rBC-containing particles, using previously published metrics. The mass ratio between non-rBC material and rBC material (MR) is calculated to determine the thickness of a hypothetical coating if the rBC and other material followed a concentric sphere model (the 'equivalent coating thickness'). The bulk MR (MR_{bulk}) was found to vary between 2-12 in winter and between 2-3 in summer. This mass-resolved mixing state is used to derive the mass-weighted mixing state index for the rBC-containing particles (χ_{rBC}). χ_{rBC} quantifies how uniformly the non-rBC material is distributed across the rBC-containing particle population, with 100% representing uniform mixing. The χ_{rBC} in Beijing varied between 55% and 70% in winter depending on the dominant air masses and χ_{rBC} was highly correlated with increased MR_{bulk} and PM$_1$ mass concentration in winter, whereas χ_{rBC} in summer varied significantly (ranging 60% - 75%) within the narrowly-distributed MR_{bulk} and was found to be independent of air mass sources. In some model treatments, it is assumed that more atmospheric ageing causes the BC to tend towards a more homogeneous mixture, but this leads to the conclusion that the MR_{bulk} may only act as a predictor of χ_{rBC} in winter. The particle morphology-independent and mass-based information on BC mixing used in this and future studies can be applied to mixing-state aware models investigating atmospheric rBC aging.

1 Introduction

Black Carbon (BC) is an important light absorbing carbonaceous component of the atmospheric particulate matter and is regarded as dominant amongst absorbing aerosols in the atmosphere (Bond and Bergstrom, 2006). Atmospheric BC particles have both a direct positive impact and semidirect impact on Earth's radiative balance (Jacobson, 2000;Bond et al., 2013;IPCC, 2013). However, the climate impact of atmospheric BC particles contains large uncertainties (Ramanathan and Carmichael, 2008;Bond et al., 2013;Riemer et al., 2019). It is known that when BC is coated with other compounds, the absorption will be enhanced due to the so-called 'lensing effect' compared to the bare BC (Jacobson, 2001;Lack and Cappa, 2010) and the magnitude of coating thickness has a significant impact on the absorption properties of BC-containing particles (Moffet and Prather, 2009). However, the optical properties of BC-containing particles vary with BC mixing state, morphology, and chemical compounds which induces large uncertainties in the calculation of the BC absorption enhancement (Cappa et al., 2012;Liu et al., 2017). A number of observations (Cappa et al., 2012;Peng et al., 2016;Liu et al., 2017;Zhang et al., 2018b) and model studies (Wu et al., 2018;Zhang et al., 2018a) suggest that the absorption enhancement ranges from 1.0 up to 3.5. Though a number of different proposed model treatments give different predictions of BC mixing state (Jacobson, 2001;Murphy et al., 2006;Péré et al., 2009), none of these give perfect agreement with atmospheric observations, either in situ or remote (Fierce et al., 2016). As the coated BC particles may act as cloud condensation nuclei (CCN) in the atmosphere, the coating thickness information of BC-containing particles can also influence the wet removal rate and thus its atmospheric lifetime and overall climate forcing potential (Kuwata et al., 2007;Schroder et al., 2015;Motos et al., 2019). Taylor et al. (2014) shows that the size distribution of BC-containing particles is important for the simulation of BC lifetime, vertical profile and transportation. The results from Liu et al. (2015) also show that the coating thickness of BC particles can largely influence their scavenging efficiency and lifetime in the clouds. The BC mixing state is especially important for polluted environments, where a combination of active sources, mixing and secondary aerosol formation mean that the BC mixing state is highly dynamic (Riemer et al., 2009). The mixing state of BC in most models remains unconstrained due to lack of measurement data, so this study aims to address this need by applying a new measurement technique to the atmosphere and offering new insight into the behaviour of BC in an important megacity.

To clearly quantify how well the BC particles are mixed in the atmosphere, the parameter "mixing state index" is applied for BC-containing particles in this study. Inspired by ecology studies (Whittaker, 1960, 1965), Riemer and West (2013) introduced a mathematical framework to quantify the aerosol mixing state. In this framework, the mixing state index (χ) is defined as the ratio between the average single particle species diversity (D_α) and the bulk particle species diversity (D_γ), and the mixing state index (χ) varies from 0% (full external mixing, i.e. all particles consist of only one species which may be different for each particle) and 100% (full internal mixing, i.e. all particles are equally composed of all species). A number of measurement studies have generated this statistic by reporting a mass fraction of different compositions through various measurement techniques. Healy et al. (2014) reported that the variation of bulk aerosols mixing state index in Paris winter is more related to

the dominated air mass source by applying the single particle aerosol mass spectrometer. Dickau et al. (2016) introduces a size and mass selection method to quantify the volatile mixing state of soot. As well as online measurements, offline microscopy techniques are also being used to retrieve species mass fractions. Bondy et al. (2018) performed a microscopy study on air samples collected from the south-eastern United States, and they found that most of the accumulation mode particles are internally mixed when the secondary organic aerosol concentration is high, and most of them are externally mixed during dust events. In this study, the mass-weighted mixing state index for rBC-containing particles (χ_{rBC}) is derived to investigate the distribution of non-rBC material across the rBC-containing particle population in Beijing. As one of the large mega-cities in China, Beijing has suffered from heavy air pollution (Yang et al., 2005) and is likely to have many factors affecting BC mixing state, which in turn has implications for both air quality and climate (Ching and Kajino, 2018). These aerosols can have a global reach (Liu et al., 2015) and as their effects may be influenced by dynamic effects near the point of emission where concentrations are highest, a polluted urban environment represents a good location to investigate these behaviours and properties.

In this study, a coupled combination of a Centrifugal Particle Mass Analyser (CPMA, Cambustion Ltd., Cambridge, UK) and a single particle soot photometer (SP2, DMT, Boulder, CO, USA) with a new inversion algorithm was applied in the field for the first time to characterise the mixing state of rBC-containing particles in Beijing. In this context, the BC is referred to as 'refractory black carbon' or rBC as an operational definition, consistent with Petzold et al. (2013). Liu et al. (2017) first introduced this morphology-independent instrument configuration to measure the mass ratio between non-rBC material and rBC material. Compared to the traditional SP2 only measurement, the significant improvement of the CPMA-SP2 method is that it can measure the non-rBC material mass directly which means no assumption is needed for non-rBC material density or its optical scattering behaviour. To clearly characterize the distribution of both rBC material and non-rBC material as part of a continuous scan (as opposed to discrete masses used previously by Liu et al. (2017)), the CPMA-SP2 results are presented in a two variable distribution by applying a novel inversion method presented by Broda et al. (2018). The concentric spheres equivalent coating thickness of rBC-containing particles and the non-rBC material distribution information across the rBC-containing particle population is derived from the measurement results, and the implication of these results are discussed.

2 Experiment details

2.1 APHH field campaign

With the aim of identifying the mixing states of rBC in a complex urban environment, an experiment was devised as part of the Air Pollution and Human Health-Beijing (APHH-Beijing) programme. The details of the wider campaign are described in Shi et al. (2018). The measurements were conducted during the APHH winter (10th Nov – 10th Dec, 2016) and summer (18th May – 25th Jun, 2017) intensive observation periods at the Institute of Atmospheric Physics (IAP) tower site. The site

(39°58′28″N, 116°22′16″E) is located in between the 3rd ring and 4th ring in the urban area of Beijing to the north of the city centre. As part of the AIRPRO and AIRPOLL joint campaign, these measurements also contribute to the better understanding of the critical pollutants and the pollution process in urban Beijing.

5 ## 2.2 Centrifugal Particle Mass Analyser (CPMA)

The CPMA sorts particles by their mass to charge ratio. The details of the CPMA have been described elsewhere (Olfert and Collings, 2005;Olfert et al., 2006). Briefly, two rotating coaxial cylindrical electrodes rotate at different angular velocities inside the CPMA. Particles of a narrow range of mass to charge ratio will exit the classifier based on a balance between electrostatic and centrifugal forces depending on the voltage difference between the electrodes and their rotational speed. The

10 average mass of the particles (m) exiting the CPMA is:

$$m = \frac{\phi e V}{\omega_c^2 r_c^2 ln\left(\frac{r_o}{r_i}\right)} \quad (1)$$

Where, e is the electronic charge (1.6×10^{-19} C), ϕ is number of charges carried by each particle, V is the voltage difference,

15 r_o is the outer cylinder radius, r_i is the inner cylinder radius, and ω_c is the rotation speed of the gas at the center of the gap between the cylinders r_c ($r_c = \frac{1}{2}(r_o + r_i)$). The charging in this instance was provided by a bipolar electrical neutralizer (MSP Corp., Shoreview, USA) that gives an equivalent charging profile to a traditional radioactive neutralizer for particles larger than 10 nm. An additional bypass flow of 1 lpm was provided in addition to the 0.1 lpm sample flow of the SP2 to minimize diffusional losses through the neutralizer and tubing.

2.3 Single Particle Soot Photometer (SP2)

The SP2 is widely used in atmospheric rBC studies (Stephens et al., 2003). It consists of four optical detectors and one Nd:YAG crystal laser with a Gaussian intensity distribution (Schwarz et al., 2010). The SP2 can detect particles with an rBC component equivalent to a spherical diameter of 70-850 nm (Liu et al., 2010;Adachi et al., 2016). The details of the SP2 algorithm in

25 Manchester is described in Liu et al. (2010) and McMeeking et al. (2010). The Manchester SP2 incandescence signal was calibrated using Aquadag black carbon particle standards (Aqueous Deflocculated Acheson Graphite, manufactured by Acheson Inc., USA) before the measurement, and the correction factor of 0.75 for ambient rBC measurement was applied (Laborde et al., 2012).

2.4 Manchester CPMA-SP2 system

A novel coupling measurement method, CPMA-SP2, has been applied to measure the non-rBC material mass among the population of rBC without morphology dependence (Liu et al., 2017). To set up the CPMA-SP2 system, the CPMA is placed upstream of the SP2 to classify particles of a nominal mass, and sequentially pass these monodisperse particles to the SP2 for analysis of the mass of rBC from the individually classified particles. When sampling with the CPMA-SP2 system, the CPMA was set to select particles from 0.3 fg up to ~ 15 fg. The CPMA performed one scan every 30 min, and it took ~20 min to complete one scan. For the remaining time, the CPMA rotation and voltage were disabled, meaning the SP2 was measuring the polydisperse aerosol measurement. A comparison between this and a bypassed configuration demonstrated that this introduced minimal losses. The CPMA-SP2 set up with mono-mass and poly-dispersed scan sequence is shown in Fig. S1.

2.5 NR-PM$_1$ (Non-refractory particulate matter with aerodynamic diameter <1 μm) measurement and back trajectory model

A High-Resolution Time-of-flight Aerodyne Mass Spectrometer (HR-ToF-AMS, Aerodyne Research Inc., USA) was used to measure the bulk aerosol non-refractory chemical compositions. The details of HR-ToF-AMS is described by DeCarlo et al. (2006). The mass concentration of the NR-PM$_1$ (Non-refractory particulate matter with aerodynamic diameter <1 μm) particle is calculated from the sum of organics, sulphate, nitrate, ammonium and chloride.

The HYSPLIT back trajectory model (Draxler and Hess, 1998) was run with the 1°×1° horizontal and vertical wind fields provided by the GDAS1 reanalysis meteorology data. The HYSPLIT model analysis was used to classify the sources of air mass influenced the measurement site, and this method is described by Liu et al. (2018b). As shown in Figure 1, the continental air mass sources are classified into five regions: Northern Plateau, Southern Plateau, Western North China Plain (NCP) and Eastern NCP.

3 Methods

3.1 CPMA-SP2 inversion

To quantify the rBC mixing state in Beijing, the CPMA-SP2 results have been applied to a new inversion method introduced by Broda et al. (2018), according to the calculations described in the supplements. The multiply charged particles are removed through the inversion process, and a two-variable distribution function is used to describe the distribution of the non-rBC material on the rBC particles:

$$\frac{\partial^2 N_{\mathrm{rBC}}}{\partial \log m_{\mathrm{p}} \partial \log m_{\mathrm{rBC}}} \quad (2)$$

where m_p is the total mass of an individual rBC-containing particle, and m_{rBC} is the mass of an individual rBC particle. N_{rBC} represents the number concentration of rBC-containing particles with their total particle mass between m_p and $m_p + dm_p$ and rBC particle mass between m_{rBC} and $m_{rBC} + dm_{rBC}$. This two-variable distribution can also be integrated to single-variable number distributions ($\frac{dN_{rBC}}{dlog m_p}$ and $\frac{dN_{rBC}}{dlog m_{rBC}}$) that are normally used in aerosol studies. An example of the original inverted two-dimensional distribution $\frac{\partial^2 N_{rBC}}{\partial log m_p \partial log m_{rBC}}$ graph retrieved from the measurement is presented in the Figure S2.

3.2 Mixing state index of rBC-containing particles calculation

Riemer and West (2013) introduced the so called "diversity parameters" to describe the particle mixing state. These parameters are based on the calculation of Shannon information entropy which is often used to quantify uncertainties, and is different from the thermodynamic entropy used in other areas (Shannon, 2001). The calculation process is described in Riemer and West (2013), and the necessary calculation process for the CPMA-SP2 results is described in the supplements. In this study, each rBC-containing particle is considered to contain two types of material: rBC material and non-rBC material. The mass fractions of rBC material and non-rBC material for each single rBC-containing particle and the bulk rBC-containing particle population that are used for the calculation are derived from the measured mass parameters. Briefly, the mixing state index for rBC-containing particles (χ_{rBC}) term can be given from:

$$\chi_{rBC} = \frac{D_\propto - 1}{D_\gamma - 1} \qquad (3)$$

Where $D_\propto$ and D_γ represent the single-particle diversity and the bulk population diversity respectively and are used to describe the effective number of species in the single particle and the population of particles. The mass-weighted parameter χ_{rBC} enables the precise quantification of the distribution of rBC material and non-rBC material mass fractions across the rBC-containing particle population. For a well-mixed situation (all the rBC-containing particles contain the same mass fraction of rBC material and non-rBC material), $D_\gamma = D_\propto = 2$, and the mixing state index $\chi_{rBC} = 100\ \%$. For a fully externally mixed situation (all the rBC-containing particles only contain the rBC material), $D_i = D_\propto = 1$, and the mixing state index χ_{rBC} will be undefined.

In this study, a high value of χ_{rBC} means that all the rBC-containing particles have the very similar rBC and non-rBC material mass fractions and is referred as 'even mixture'. While a low value of χ_{rBC} means the distribution of rBC and non-rBC material mass fractions is uneven across the rBC-containing particles population and is referred as 'uneven mixture'.

3.3 CPMA-SP2 two variable distribution extrapolation

As introduced in the previous section, the CPMA-SP2 system measurement range set for this measurement campaign is up to $m_p = 15$ fg, which is roughly between 0.25 μm and 0.28 μm in equivalent volume diameter for typical urban rBC-containing particles, based on studies in other cities. However, during certain periods throughout the winter campaign, the distribution unexpectedly extended to larger sizes outside of this range, meaning the overall rBC population was not completely captured by the measurement data. Some other studies regarding to the rBC-containing particle size distribution in China (Gong et al., 2016;Wu et al., 2017;Zhang et al., 2018b) are in agreement that the volume diameter of rBC-containing particles is larger than the largest CPMA selected size set in this study. To better quantify the bulk rBC mixing states and overcome the measurement range limitation, the number concentration of rBC-containing particles is extrapolated beyond the measurement range. From the previous CPMA-SP2 results by Liu et al. (2017), the number of distribution can be assumed as log-normal. Hence, the inversion results are extrapolated up to m_p around 300 fg, which is about 0.8 μm in equivalent volume diameter, by fitting the measured results with the simulated distribution function, generated from the superposition of two lognormal distributions. Further details of the extrapolation process are presented in the supplementary material. Briefly, the number distribution for m_p ($\frac{dN_{rBC}}{d\log m_p}$) is extrapolated based on the fitted distribution function. Two methods were then attempted to extrapolate the two-dimensional distribution $\frac{\partial^2 N_{rBC}}{\partial \log m_p \partial \log m_{rBC}}$, and critically compared with a view to determining the optimal method. One was based on fitting the two-variable distribution distribution as a function of m_{rBC} (Fit m_{rBC} Method), and other based on fitting the two-variable distribution as a function of the mass ratio between the m_p and m_{rBC} (Fit Ratio Method):

$$\left. \frac{\partial^2 N_{rBC}}{\partial \log m_p \partial \log m_{rBC}} \right|_{\text{Fit mrBC},(i,j)} = R_i \cdot \left(a_1 \cdot \exp\left(-\left(\frac{\log(m_{rBC,j}) - b_1}{c_1} \right) \right) + a_2 \cdot \exp\left(-\left(\frac{\log(m_{rBC,j}) - b_2}{c_2} \right) \right) \right) \quad (4)$$

$$\left. \frac{\partial^2 N_{rBC}}{\partial \log m_p \partial \log m_{rBC}} \right|_{\text{Fit Ratio},(i,j)} = R_i \cdot \left(a_1 \cdot \exp\left(-\left(\frac{\log(m_{p,i}/m_{rBC,j}) - b_1}{c_1} \right) \right) + a_2 \cdot \exp\left(-\left(\frac{\log(m_{p,i}/m_{rBC,j}) - b_2}{c_2} \right) \right) \right) \quad (5)$$

While $\left. \frac{\partial^2 N_{rBC}}{\partial \log m_p \partial \log m_{rBC}} \right|_{(i,j)}$ represents the number concentration of two variable distribution at m_p bin i and m_{rBC} bin j; R_i is the ratio between the rBC-containing particles number concentration at the extrapolated m_p bin i and the number concentration at the measured largest m_p bin (the bin with $m_p = 15$ fg), a_1, b_1, c_1, a_2, b_2, c_2 are all the parameters for the distribution function.

To validate the reliability of the extrapolation, the total rBC mass concentration from the CPMA-SP2 extrapolations are compared with the SP2 data obtained during polydisperse sampling (shown in Figure 2). For the polluted periods where large rBC-containing particles exist, the Fit Ratio method may overestimate the extrapolated rBC material size, and as a result, the

extrapolated rBC mass is significantly higher than the SP2 only results for the polluted periods. The comparison of Fit Ratio and Fit m_{rBC} extrapolation methods shown in Figure 2(a) illustrates that the Fit m_{rBC} method is closer to the rBC mass concentration measured by the SP2 only method. For the summer results shown in Figure 2(b), the extrapolation results for the two methods are similar because the rBC-containing particles were smaller and therefore the extrapolation was less necessary.

In general, the Fit m_{rBC} method was found to better approximate the total rBC mass compared to the Fit Ratio method. Therefore, the results in this study are extrapolated by the Fit m_{rBC} method.

4 Results and discussion

4.1 APHH campaign overview and CPMA-SP2 two-variable distributions

Figure 3 presents an overview of rBC and NR-PM$_1$ mass concentration for the whole winter and summer campaign. The rBC and NR-PM$_1$ mass concentration varied significantly in winter, the rBC mass concentration increased to beyond $10\ \mu\text{g}\cdot\text{m}^{-3}$ while the NR-PM$_1$ mass concentration increased above $300\ \mu\text{g}\cdot\text{m}^{-3}$ during the polluted periods. In contrast, the rBC and NR-PM$_1$ mass concentration reduced significantly during the light pollution periods. Compared to the winter periods, the rBC mass concentration varied less significantly in summer, and the peak of rBC mass concentration and NR-PM$_1$ mass concentration is lower. The rBC mass concentration reached a peak of around $4\ \mu\text{g}\cdot\text{m}^{-3}$ while the NR-PM$_1$ mass concentration reached a peak of around $100\ \mu\text{g}\cdot\text{m}^{-3}$.

Figure 4 shows the two-dimensional distribution $\frac{\partial^2 N_{\text{rBC}}}{\partial \log m_{\text{p}} \partial \log m_{\text{rBC}}}$ graph which presents the measured BC mixing state. To improve the signal-to-noise ratio of the data, the measured CPMA-SP2 data have been averaged over 3-hour periods. According to the measurement results from winter campaign period, three types of mixing state distribution under three different pollution levels were observed and these three types of pollutions are: Heavy Pollution (NR-PM$_1$ greater than 200 $\mu\text{g}\cdot\text{m}^{-3}$), Moderate Pollution (NR-PM$_1$ between 100 and 200 $\mu\text{g}\cdot\text{m}^{-3}$), and Light Pollution (NR-PM$_1$ less than 100 $\mu\text{g}\cdot\text{m}^{-3}$). These representative distribution under different pollution levels are shown in Figure 4(a–c). Figure 4(a) shows high concentrations of rBC-containing particles with both large rBC material and non-rBC material were observed under heavy haze (fog) pollution conditions in the morning of 4$^{\text{th}}$ Dec. During that day, a surface low pressure persisted in Beijing and its surrounding area, so air pollution accumulated to high concentrations. For the moderate pollution period shown in Figure 4(b), a large number of rBC-containing particles with smaller amounts of rBC material and non-rBC material were observed. The period of light pollution shown in Figure 4(c) has the smallest number concentration of rBC-containing particles among all the three pollution types but the shape of the two-variable distribution is similar to the moderate pollution period in that most of the rBC-containing particles were smaller than 10 fg and rBC particles with a relatively large non-rBC material fraction were

rare. As no highly polluted events comparable to winter were observed in summer, the $\frac{\partial^2 N_{rBC}}{\partial \log m_p \partial \log m_{rBC}}$ distribution in summer does not show as much variation during the whole campaign period - one example is shown in the Figure 4(d). It appears that the $\frac{\partial^2 N_{rBC}}{\partial \log m_p \partial \log m_{rBC}}$ distribution in summer is similar to the distribution for moderate or light pollution periods in winter.

5   The single variable size distribution results from the integration of $\frac{\partial^2 N_{rBC}}{\partial \log m_p \partial \log m_{rBC}}$ are displayed in Figure 5. The volume equivalent diameter for rBC-containing particles (D_p) and the rBC material (D_c) is also calculated by assuming a density of 1.2 g/cm^3 for rBC-containing particles and a density of 1.8 g/cm^3 for rBC material for better comparison with other studies based on aerodynamic diameter. For the m_p number concentration size distribution ($\frac{dN_{rBC}}{d\log m_p}$) shown in Figure 5(a), the mode particle size is between 2 fg and 10 fg for the light pollution and moderate pollution periods, while for the heavy pollution

10   period there is a large increase in the number concentration for rBC-containing particles larger than 5 fg. The number concentration size distribution for the m_{rBC} ($\frac{dN_{rBC}}{d\log m_{rBC}}$) shown in Figure 5(b) indicates that there is an increase in the number concentration for the rBC-containing particles with relatively large rBC material (with m_{rBC} larger than 1 fg) during the heavy pollution period in winter.

15   **4.3 Mass ratio between non-rBC material and rBC material**

The concentric spheres equivalent coating thickness information is presented through the mass ratio (MR) parameter which is derived from the CPMA-SP2 inversion results. The *MR* parameter defined here follows the definition of Liu et al. (2017), which is given by:

20    $$MR_i = \frac{m_{\text{non-BC},i}}{m_{\text{rBC},i}} = \frac{m_{p,i} - m_{\text{rBC},i}}{m_{\text{rBC},i}} \qquad (6)$$

where MR_i is the mass ratio for rBC-containing particle i, and $m_{\text{non-rBC}}$ is the non-rBC material within rBC-containing particle i, $m_{p,i}$ and $m_{rBC,i}$ are the mass of the rBC-containing particle i and the mass of the rBC material for rBC-containing particle i respectively. The traditional SP2 only method calculates MR by applying measured optical properties through the

25   leading edge only (LEO) technique, and assumptions regarding the refractive indices and morphology are needed to determine the bulk concentric spheres equivalent coating thickness (Gao et al., 2007;Liu et al., 2014;Broda et al., 2018). The CPMA-SP2 method, however, is able to quantify the mass parameters more directly and without LEO fitting or a scattering inversion, therefore the MR measured by CPMA-SP2 can be considered to be much more accurate. The bulk MR (MR_{bulk}) measured by CPMA-SP2 is calculated as follows:

$$MR_{bulk} = \frac{\int \frac{dM_p}{dlogm_p}dlogm_p}{\int \frac{dM_{rBC}}{dlogm_{rBC}}dlogm_{rBC}} = \frac{\iint \frac{\partial^2 N_{rBC}}{\partial logm_p \partial logm_{rBC}}m_p dlogm_{rBC}dlogm_p}{\iint \frac{\partial^2 N_{rBC}}{\partial logm_p \partial logm_{rBC}}m_{rBC}dlogm_{rBC}dlogm_p} - 1 \qquad (7)$$

where M_p and M_{rBC} are the total mass concentration for rBC-containing particles and rBC particles respectively. The comparison between MR_{bulk} from the CPMA-SP2 method and the SP2-only method is shown in Figure 6. The MR_{bulk} from the SP2-only method is derived by applying the SP2 LEO fitting method to rBC-containing particles with D_p in the range of 0.08 ~ 0.8 μm, and D_c in the range of 0.08 ~ 0.55 μm. The MR_{bulk} from the CPMA-SP2 method shows a good correlation with the SP2-only method during the summer period and the winter period. Despite a slight lower MR_{bulk} observed from the SP2-only method, the MR_{bulk} results from the two methods are generally close.

The CPMA-SP2 MR_{bulk} time series for winter and summer are presented in Figure 7. A significant increase was observed during the winter heavy pollution period, and the MR_{bulk} reached a maximum of 10 on December 4th. During low pollution periods the rBC particles had a lower MR_{bulk} around 2. According to the source apportionment work during the same study by Liu et al. (2018a) and Wang et al. (2019), around 64% of organic components within the rBC-containing particles were from primary sources in winter. These sources may also emit non-rBC material externally mixed with rBC. During the heavy pollution period in winter, a significant enhancement of secondary organic aerosol was observed (Wang et al., 2019). Figure 4 showed that during the highly polluted period, there were large numbers of rBC-containing particles with m_{rBC} between 1 fg and 10 fg. These rBC-containing particles with large m_{rBC} mostly originated from the southern Plateau based on the back-trajectory analysis in Fig. 10a, and Liu et al. (2018a) suggested that they may be from coal burning. High pollution tends to introduce increased concentrations of gas precursors promoting the condensation of secondary material, and the higher overall particulate concentration promotes coagulation, particularly at the top of the boundary layer where the high humidity causes particles to grow further. Both condensation and coagulation will lead to more efficient mixing of rBC and increased MR_{bulk}. In contrast, during the lightly polluted periods, the fractions of non-rBC material within the rBC-containing particle population were much lower. The relatively cleaner air masses from Northern Plateau dominated most of the light pollution periods (Liu et al., 2018a). With the absence of high absolute non-rBC material concentrations, the rBC-containing particles were externally mixed or with lower fraction of non-rBC material.

Figure 7 shows that the MR_{bulk} in summer varied between 1 and 2.7 with several moderate MR_{bulk} values (MR_{bulk} >2), which was generally lower than in winter. Compared to the winter periods, the source apportionment shows that secondary material contributed more to the total organic aerosol species within the rBC-containing particles (Xie et al., 2019; Wang et al., 2019).

The MR_{bulk} frequency distribution is presented in Figure 8. Most of the rBC-containing particles contained a small fraction of non-rBC material with the MR_{bulk} less than 2 in both winter and summer. The range of MR_{bulk} values was also much broader in winter compared to the summer period. Some rBC-containing particles containing a large fraction of non-rBC material ($MR_{bulk} > 3$) were observed in winter while no such particles were found during the summer period. In general, the MR_{bulk} frequency distribution from the CPMA-SP2 and SP2-only methods are similar.

A CPMA-SP2 two-variable distribution is able to present detailed single rBC-containing particle concentric spheres equivalent coating thickness information. The MR_i can be derived to quantify the concentric spheres equivalent coating thickness on each rBC-containing particle. Liu et al. (2017) stated that rBC-containing particles with MR_i lower than 1.5 are typical for traffic emissions while an MR greater than 3 is typical for biomass burning emissions. The rBC mass fraction under different MR_i level classifications is presented in Figure 9. Comparing the summer results with the winter results, the fraction of rBC-containing particles with a tiny fraction of non-rBC material ($MR_i \sim 0$) and rBC-containing particles with a moderate fraction of non-rBC material ($1.5 \leq MR_i < 3$) is similar. The mass fraction varied slightly around 20% for uncoated rBC-containing particles at both summer and winter campaign periods. The rBC-containing particles with a large fraction of non-rBC material ($MR_i \geq 3$) accounted for a higher fraction in winter, especially for the heavy haze periods between the 3rd and 5th of December. The significant enhancement of the fraction of rBC-containing particles with $MR_i \geq 3$ was more likely related to the increase of the fraction of secondary components during the heavily polluted period in winter (Wang et al., 2019). The rBC-containing particles with a small fraction of non-rBC material ($0 < MR_i < 1.5$) accounted for a large portion (around 60%) during the lightly pollution periods in winter and occurred most of the time in summer. These rBC-containing particles with much lower MR_i were likely to be generated from the consumption of fossil fuel (Liu et al., 2017;Liu et al., 2018a).

4.4 Entropy parameters and rBC mixing state

Derived from the CPMA-SP2 inversions, the bulk diversity (D_γ) and the mixing state index for rBC-containing particles (χ_{rBC}) results shown in Figure 10 illustrate the variation of BC mixing state for the whole APHH campaign period. As the CPMA-SP2 system only detects the rBC-containing particles, therefore the number of species set here is 2; the rBC and non-rBC material. To reiterate, this metric should be taken as the level of homogeneity of rBC mixing state amongst the rBC-containing particles.

χ_{rBC} varied around 62% between 10th Nov and 21st Nov. A decrease of χ_{rBC} was observed between 19th and 20th Dec which indicates a period of more externally mixed rBC. Apart from some minor χ_{rBC} spikes, the mixing state of rBC-containing particles remained unchanged between 10th Nov and 21st Nov. Whereas for the results between 1st Dec and 6th Dec, χ_{rBC} and D_γ varied dramatically. After the polluted period on 30th Nov, a light pollution period occurred on 1st Dec and χ_{rBC} decreased

rapidly to below 60%. When the haze formed between 2nd Dec and 4th Dec, χ_{rBC} increased gradually. On contrast, D_γ decreased significantly during this heavy polluted period which was mainly caused by the thick non-rBC material on the rBC material leading to a reduction of rBC material mass fraction percentage. The haze subsided after χ_{rBC} reaches the peak of around 70% on 4th Dec, another light pollution period appeared and χ_{rBC} and D_γ resumes to the value before the haze. For the

5 moderate polluted period between 6th and 7th Dec, χ_{rBC} reached another peak of around 68%, and the increase of MR_{bulk} led D_γ to decrease to around 1.5.

To investigate the mixing state of smaller rBC-containing particles, the mixing state index at smaller m_p is also calculated, shown in Figure 10. The χ_{rBC} at $m_p \leq 15$ fg and $m_p \leq 5$ fg is shown to be higher than the bulk χ_{rBC}, indicating that the rBC

10 material was more evenly distributed among rBC-containing particles at smaller sizes. For most of the winter period, the trend of χ_{rBC} at $m_p \leq 15$ fg and $m_p \leq 5$ fg was similar to the trend of bulk χ_{rBC}. However, during the heavy pollution period between 3rd Dec and 4th Dec, the χ_{rBC} at $m_p \leq 5$ fg decreased slightly suggesting that there was a relatively uneven distribution of rBC material and non-rBC material mass fractions for the smaller rBC-containing particles. During summer, the χ_{rBC} at $m_p \leq 15$ fg and $m_p \leq 5$ fg was closer to the bulk χ_{rBC} because of rBC-containing particles in summer being

15 smaller and most of the rBC-containing particles having smaller MR_i.

The mixing state of rBC-containing particles can be also associated with the air mass sources, and the relationship between the major air mass source, MR and rBC mixing state is further explored further in Figure 11. The winter characterisation result is shown in Figure 10(a) and Figure 11(a). Among all the air mass sources, Plateau South and Western NCP were considered

20 to represent the polluted air masses from which aged rBC-containing particles with larger MR_i were transported during this period. When higher χ_{rBC} (between 60% and 75%) and MR_{bulk} values (between 2 and 12) were observed the Plateau South air mass periods dominated. When Local air mass and Plateau North air mass accounted for more fractions, the presences of rBC-containing particles with smaller MR_i contributed to the significant increase of D_γ values and rapid decrease of χ_{rBC} and MR_{bulk} values. For example, the reduction of rBC-containing particles internal mixture on 30th Nov and 5th Dec can be

25 associated with a relative clean Plateau North air mass. This evolution during the winter period agrees with the findings from Paris of Healy et al. (2014), who found that when considering the mixing state of bulk aerosol mass (which considered multiple non-rBC species) there was a trend towards more homogenous mixing when polluted air masses dominate compared to the local and clean marine air mass periods.

30 For the summer period shown in Figure 10(b), χ_{rBC} varied between 60% and 75%. As the MR_{bulk} was lower in summer, the mass fraction of rBC material and the mass fraction of non-rBC material was closer within the bulk population, hence a slightly higher D_γ was observed in summer. Though the MR_{bulk} and the rBC mass concentration was not as high as that in winter, sharp decreases in D_γ together with the increase of χ_{rBC} still occurred occasionally in summer which indicate that some rBC-

containing particles with moderate non-rBC material was observed. Unlike the winter campaign period, the back-trajectory results in summer shown in Figure 11(b) do not show a significant association between mixing state parameters and air mass origin.

5   **4.6 Discussion**

In order to investigate which other parameters may act as a predictor for mixing state, Figure 12 shows the variation of χ_{rBC} in both summer and winter against (a) NR-PM$_1$ and rBC mass concentration, and (b) MR_{bulk}. There was a positive correlation between the variation of χ_{rBC} and the variation of MR_{bulk} in winter as rBC-containing particles with larger non-rBC material (larger MR_{bulk}) tended to exhibit a more even mixture during the winter campaign period. For the summer period, no such

10   positive correlation was found. Although the rBC-containing particles did not contain a large fraction of non-rBC material in summer, and the pollution level was lower, there was significant variation of χ_{rBC} which indicates that the distribution of rBC and non-rBC material mass fractions among the rBC-containing particles varies in a narrow range of lower MR_{bulk}. This indicates that higher MR_{bulk} can be related to increased levels of a more even mixture of rBC-containing particles in winter, while the MR_{bulk} metric cannot be used to predict the variation of χ_{rBC} in summer.

Comparing the two seasons, there was more diversity in the distribution of rBC mixing state in summer than in winter under similar MR_{bulk} or similar NR-PM$_1$ and rBC mass concentrations. About 30% of the experimental period in summer had χ_{rBC} over 70%, however this fraction was almost absent in winter. This means although the pollution was low in summer, a more homogenous distribution of non-rBC material was present.

As χ_{rBC} is a mass-weighted parameter, it is dominated by the larger rBC-containing particles. During the heavy pollution period in winter, there was generally more particulate matter, so the non-rBC materials have a higher probability of coagulating with or condensing on primary rBC, resulting in the relatively higher amount of non-rBC material detected in winter. The rBC particles with a higher MR_i contributed most to the rBC mass concentration during the heavy polluted periods (shown in Figure

25   9), and the fraction of the secondary non-rBC material within rBC-containing particles increased with pollution level (Wang et al., 2019). These large rBC-containing particles with a large fraction of non-rBC material dominated the total rBC-containing particle mass and showed a higher χ_{rBC} value. This increasing trend of χ_{rBC} was shown to correspond to the MR_{bulk} and NR-PM$_1$ level, and this means the higher pollution will be associated with enhanced non-rBC material and a similar mixing state for most rBC-containing particles in winter.

30
During the lighter pollution periods, most of the rBC-containing particles had a lower MR_i, and a lower MR_{bulk} was present. A lower χ_{rBC} was present when MR_{bulk} or the pollution level was lower in winter. One reason is that though the MR_{bulk} is

lower, there were still some relatively large rBC-containing particles with a large or moderate MR_i, which were not sufficient to dominate the overall rBC-containing particle mass concentration or overall χ_{rBC} during the light pollution periods. A significant difference was thus observed between the χ_{rBC} for small rBC-containing particles (at $m_p \leq 5$ fg) and the bulk χ_{rBC}. The other reason for the uneven distribution of non-rBC material and rBC material mass fractions may be that the appearance of non-rBC material in rBC-containing particles is being limited. There were more rBC-containing particles with little non-rBC material during this period, compared to the moderate or heavy pollution periods in winter. Therefore, the non-rBC material and rBC material mass fractions tended to be unevenly distributed among rBC-containing particles and the χ_{rBC} shows a lower value.

As there were fewer large rBC-containing particles in summer, the bulk χ_{rBC} result is close to the χ_{rBC} result of smaller rBC-containing particles, and the bulk χ_{rBC} is generally higher than the winter period for most of the time. This could be through a lower diversity of sources during certain periods and/or a difference in atmospheric processes that leads to a uniform condensation of secondary material without significantly raising MR_{bulk}. In summer, the concentrations of primary aerosols are lower compared to winter, and secondary organic aerosols (SOAs) contribute a larger fraction to the total organic aerosols (OA) in Beijing (Sun et al., 2018;Hu et al., 2016). Previous studies show that an internal mixture would be expected for BC associated with a larger secondary fraction (Krasowsky et al., 2018;Bondy et al., 2018), but the lower overall pollution levels in summer limited the formation of large rBC-containing particles. This may cause the large variation of χ_{rBC} in summer.

Results comparing both seasons suggest that the increase of non-rBC material with MR_{bulk} above 4 could lead to a more even distribution of rBC and non-rBC material ($\chi_{rBC} > 60\%$), as indicated by the winter results. In contrast, during summer the χ_{rBC} had a larger variation and an even mixture for rBC-containing particles was still possible when MR_{bulk} and the overall pollution level was lower.

5 Implications for the future studies

The CPMA-SP2 together with a new inversion method are capable of exploring ambient BC mixing state in a way not previously possible. The detailed two variable distribution is able to retrieve the mixing state information on a single particle level. For future studies, the detailed two variable distribution results from the CPMA-SP2 can be directly compared with mixing-state aware models such as GLOMAP (Mann et al., 2010) and the particle resolved model PartMC-MOSAIC (Riemer et al., 2009) when simulating the behaviour of BC in polluted plumes. Some modelling studies have suggested that large uncertainties of BC atmospheric lifetime result from uncertainties in the scavenging efficiency (e.g. Myhre and Samset (2015)). The processes of activation and impaction scavenging are partly dictated by the overall size and soluble fraction of the rBC-containing particles, which would manifest in the data presented here. However, while some models carry this information

(e.g. 'hydrophobic' vs 'hydrophilic' BC in GLOMAP) this is poorly constrained partly because of the lack of observations that can resolve this (Taylor et al., 2014). In general, more detailed non-rBC material information (*MR* results) and single-particle level mixing state information presented in our study can contribute to future studies concerning BC lifetime and transportation to help to constrain the simulations (Bond et al., 2013;Fierce et al., 2017).

6 Conclusions

In this study, the combination of a centrifugal particle mass analyser (CPMA) and a single particle soot photometer (SP2), has been applied to the investigation of mixing state of refractory Black Carbon (rBC)-containing particles in urban Beijing. A novel CPMA-SP2 inversion algorithm is able to present the detailed two-variable number distribution as a function of rBC mass and total rBC-containing particle mass. As the CPMA-SP2 system directly measures the particle mass, more accurate mass ratio (MR) results for the rBC-containing particles are reported. With the detailed inversion metric results, the mixing state index (χ_{rBC}) is derived to quantify the distribution rBC and non-rBC material mass fractions within the population of rBC-containing particles. The measurement results show that the measured bulk MR (MR_{bulk}) during the winter campaign period varied significantly from around 2 to 12, while the χ_{rBC} value varied between 55% and 70%. The highest MR_{bulk} values were associated with the haze polluted periods in winter, and the χ_{rBC} value reached higher values under these conditions (over 65%), which illustrated there was a more even distribution of rBC and non-rBC material mass fractions during this period. This result shows that higher pollution levels will increase the non-rBC material in rBC-containing particles and a promote more homogenous distribution of non-rBC material and rBC material in winter. These results further imply that the MR_{bulk} may be a good predictor of χ_{rBC} in this season. Meanwhile, the back-trajectory analysis indicates that polluted air from Southern Plateau dominated the aged rBC-containing particles in Beijing during winter. For the summer campaign period, the MR_{bulk} varied between 2 and 3. The χ_{rBC} varied between 60% and 75% but was found to be independent of MR_{bulk}. The slightly higher χ_{rBC} in summer indicates that a more even distribution of rBC and non-rBC material mass fractions, which may be caused by higher availability of secondary material. However, a large fraction of non-rBC material within the rBC-containing particle population (large MR_{bulk}) was not favoured, due to the lack of heavily polluted events in summer, and further no apparent relationship was found between the rBC-containing particle mixing state and air mass sources. The observations presented here have implications for detailed models of BC, its optical properties and its atmospheric lifecycle, necessary to assess its local and global impacts. For models that consider mixing state, the methods and results discussed here can better describe the BC mixing state which may offer new insights and contribute to improvements in the accuracy of simulations.

30

Data availability

Processed SP2 data is available through the APHH project archive at the Centre for Environmental Data Analysis (http://data.ceda.ac.uk/badc/aphh/data/beijing/). Raw data is archived at the University of Manchester and is available on request.

Contribution

D.L., J.D.A. and J.O. designed the research; C.Y., D.L., J.D.A., R.J., H.C., Y.S. and P.F. performed experiments; K.B. and J.O. provided the initial inversion code; C.Y. adapted the inversion code and performed the CPMA-SP2 data analysis; D.L. performed the initial SP2 data processing and HYSPLIT runs; Y.S. analysed the NR-PM$_1$ data; C.Y., D.L. and J.D.A. wrote the paper.

Acknowledgments

This work was supported through the UK Natural Environment Research Council (grant refs. NE/N007123/1, NE/N00695X/1) and the National Natural Science Foundation of China (grant nos. 41571130024, 41571130034 and 21777073).

Competing interests: The authors declare that they have no conflict of interest

References

Adachi, K., Moteki, N., Kondo, Y., and Igarashi, Y.: Mixing states of light-absorbing particles measured using a transmission electron microscope and a single-particle soot photometer in Tokyo, Japan, Journal of Geophysical Research: Atmospheres, 121, 9153-9164, 10.1002/2016jd025153, 2016.

Bond, T. C., and Bergstrom, R. W.: Light Absorption by Carbonaceous Particles: An Investigative Review, Aerosol Science and Technology, 40, 27-67, 10.1080/02786820500421521, 2006.

Bond, T. C., Doherty, S. J., Fahey, D. W., Forster, P. M., Berntsen, T., DeAngelo, B. J., Flanner, M. G., Ghan, S., Kärcher, B., Koch, D., Kinne, S., Kondo, Y., Quinn, P. K., Sarofim, M. C., Schultz, M. G., Schulz, M., Venkataraman, C., Zhang, H., Zhang, S., Bellouin, N., Guttikunda, S. K., Hopke, P. K., Jacobson, M. Z., Kaiser, J. W., Klimont, Z., Lohmann, U., Schwarz, J. P., Shindell, D., Storelvmo, T., Warren, S. G., and Zender, C. S.: Bounding the role of black carbon in the climate system: A scientific assessment, Journal of Geophysical Research: Atmospheres, 118, 5380-5552, 10.1002/jgrd.50171, 2013.

Bondy, A. L., Bonanno, D., Moffet, R. C., Wang, B., Laskin, A., and Ault, A. P.: The diverse chemical mixing state of aerosol particles in the southeastern United States, Atmospheric Chemistry and Physics, 18, 12595-12612, 10.5194/acp-18-12595-2018, 2018.

Broda, K. N., Olfert, J. S., Irwin, M., Schill, G. P., McMeeking, G. R., Schnitzler, E. G., and Jäger, W.: A novel inversion method to determine the mass distribution of non-refractory coatings on refractory black carbon using a centrifugal particle mass analyzer and single particle soot photometer, Aerosol Science and Technology, 1-12, 10.1080/02786826.2018.1433812, 2018.

Cappa, C. D., Onasch, T. B., Massoli, P., Worsnop, D. R., Bates, T. S., Cross, E. S., Davidovits, P., Hakala, J., Hayden, K. L., and Jobson, B. T.: Radiative absorption enhancements due to the mixing state of atmospheric black carbon, Science, 337, 1078-1081, 2012.

Ching, J., and Kajino, M.: Aerosol mixing state matters for particles deposition in human respiratory system, Scientific Reports, 8, 8864, 10.1038/s41598-018-27156-z, 2018.

DeCarlo, P. F., Kimmel, J. R., Trimborn, A., Northway, M. J., Jayne, J. T., Aiken, A. C., Gonin, M., Fuhrer, K., Horvath, T., Docherty, K. S., Worsnop, D. R., and Jimenez, J. L.: Field-Deployable, High-Resolution, Time-of-Flight Aerosol Mass Spectrometer, Analytical Chemistry, 78, 8281-8289, 10.1021/ac061249n, 2006.

Dickau, M., Olfert, J., Stettler, M. E. J., Boies, A., Momenimovahed, A., Thomson, K., Smallwood, G., and Johnson, M.: Methodology for quantifying the volatile mixing state of an aerosol, Aerosol Science and Technology, 50, 759-772, 10.1080/02786826.2016.1185509, 2016.

Draxler, R. R., and Hess, G. D.: An overview of the HYSPLIT_4 modelling system for trajectories, Australian meteorological magazine, 47, 295-308, 1998.

Fierce, L., Bond, T. C., Bauer, S. E., Mena, F., and Riemer, N.: Black carbon absorption at the global scale is affected by particle-scale diversity in composition, Nat Commun, 7, 12361, 10.1038/ncomms12361, 2016.

Fierce, L., Riemer, N., and Bond, T. C.: Toward Reduced Representation of Mixing State for Simulating Aerosol Effects on Climate, Bulletin of the American Meteorological Society, 98, 971-980, 10.1175/bams-d-16-0028.1, 2017.

Gao, R. S., Schwarz, J. P., Kelly, K. K., Fahey, D. W., Watts, L. A., Thompson, T. L., Spackman, J. R., Slowik, J. G., Cross, E. S., Han, J. H., Davidovits, P., Onasch, T. B., and Worsnop, D. R.: A Novel Method for Estimating Light-Scattering Properties of Soot Aerosols Using a Modified Single-Particle Soot Photometer, Aerosol Science and Technology, 41, 125-135, 10.1080/02786820601118398, 2007.

Gong, X., Zhang, C., Chen, H., Nizkorodov, S. A., Chen, J., and Yang, X.: Size distribution and mixing state of black carbon particles during a heavy air pollution episode in Shanghai, Atmospheric Chemistry and Physics, 16, 5399-5411, 10.5194/acp-16-5399-2016, 2016.

Healy, R. M., Riemer, N., Wenger, J. C., Murphy, M., West, M., Poulain, L., Wiedensohler, A., O'Connor, I. P., McGillicuddy, E., Sodeau, J. R., and Evans, G. J.: Single particle diversity and mixing state measurements, Atmospheric Chemistry and Physics, 14, 6289-6299, 10.5194/acp-14-6289-2014, 2014.

Hu, W., Hu, M., Hu, W., Jimenez, J. L., Yuan, B., Chen, W., Wang, M., Wu, Y., Chen, C., Wang, Z., Peng, J., Zeng, L., and Shao, M.: Chemical composition, sources, and aging process of submicron aerosols in Beijing: Contrast between summer and winter, Journal of Geophysical Research: Atmospheres, 121, 1955-1977, 10.1002/2015jd024020, 2016.

IPCC: Annex I: Atlas of Global and Regional Climate Projections in: Climate Change 2013: The Physical Science Basis. Contribution of Working Group I to the Fifth Assessment Report of the Intergovernmental Panel on Climate Change, edited by: Stocker, T. F., Qin, D., Plattner, G.-K., Tignor, M., Allen, S. K., Boschung, J., Nauels, A., Xia, Y., Bex, V., and Midgley, P. M., Cambridge University Press, Cambridge, United Kingdom and New York, NY, USA, 1311–1394, 2013.

Jacobson, M. Z.: A physically-based treatment of elemental carbon optics: Implications for global direct forcing of aerosols, Geophysical Research Letters, 27, 217-220, 10.1029/1999gl010968, 2000.

Jacobson, M. Z.: Strong radiative heating due to the mixing state of black carbon in atmospheric aerosols, Nature, 409, 695, 10.1038/35055518, 2001.

Krasowsky, T. S., McMeeking, G. R., Sioutas, C., and Ban-Weiss, G.: Characterizing the evolution of physical properties and mixing state of black carbon particles: from near a major highway to the broader urban plume in Los Angeles, Atmospheric Chemistry and Physics, 18, 11991-12010, 10.5194/acp-18-11991-2018, 2018.

Kuwata, M., Kondo, Y., Mochida, M., Takegawa, N., and Kawamura, K.: Dependence of CCN activity of less volatile particles on the amount of coating observed in Tokyo, Journal of Geophysical Research, 112, 10.1029/2006jd007758, 2007.

Laborde, M., Mertes, P., Zieger, P., Dommen, J., Baltensperger, U., and Gysel, M.: Sensitivity of the Single Particle Soot Photometer to different black carbon types, Atmospheric Measurement Techniques, 5, 1031-1043, 10.5194/amt-5-1031-2012, 2012.

Lack, D. A., and Cappa, C. D.: Impact of brown and clear carbon on light absorption enhancement, single scatter albedo and absorption wavelength dependence of black carbon, Atmospheric Chemistry and Physics, 10, 4207-4220, 10.5194/acp-10-4207-2010, 2010.

Liu, D., Flynn, M., Gysel, M., Targino, A., Crawford, I., Bower, K., Choularton, T., Jurányi, Z., Steinbacher, M., Hüglin, C., Curtius, J., Kampus, M., Petzold, A., Weingartner, E., Baltensperger, U., and Coe, H.: Single particle characterization of black carbon aerosols at a tropospheric alpine site in Switzerland, Atmospheric Chemistry and Physics, 10, 7389-7407, 10.5194/acp-10-7389-2010, 2010.

Liu, D., Allan, J. D., Young, D. E., Coe, H., Beddows, D., Fleming, Z. L., Flynn, M. J., Gallagher, M. W., Harrison, R. M., Lee, J., Prevot, A. S. H., Taylor, J. W., Yin, J., Williams, P. I., and Zotter, P.: Size distribution, mixing state and source apportionment of black carbon aerosol in London during wintertime, Atmospheric Chemistry and Physics, 14, 10061-10084, 10.5194/acp-14-10061-2014, 2014.

Liu, D., Quennehen, B., Darbyshire, E., Allan, J. D., Williams, P. I., Taylor, J. W., Bauguitte, S. J. B., Flynn, M. J., Lowe, D., Gallagher, M. W., Bower, K. N., Choularton, T. W., and Coe, H.: The importance of Asia as a source of black carbon to the European Arctic during springtime 2013, Atmospheric Chemistry and Physics, 15, 11537-11555, 10.5194/acp-15-11537-2015, 2015.

Liu, D., Whitehead, J., Alfarra, M. R., Reyes-Villegas, E., Spracklen, Dominick V., Reddington, Carly L., Kong, S., Williams, Paul I., Ting, Y.-C., Haslett, S., Taylor, Jonathan W., Flynn, Michael J., Morgan, William T., McFiggans, G., Coe, H., and Allan, James D.: Black-carbon absorption enhancement in the atmosphere determined by particle mixing state, Nature Geoscience, 10, 184-188, 10.1038/ngeo2901, 2017.

Liu, D., Joshi, R., Wang, J., Yu, C., Allan, J. D., Coe, H., Flynn, M. J., Xie, C., Lee, J., Squires, F., Kotthaus, S., Grimmond, S., Ge, X., Sun, Y., and Fu, P.: Contrasting physical properties of black carbon in urban Beijing between winter and summer, Atmos. Chem. Phys. Discuss., 2018, 1-30, 10.5194/acp-2018-1142, 2018a.

Liu, D., Taylor, J. W., Crosier, J., Marsden, N., Bower, K. N., Lloyd, G., Ryder, C. L., Brooke, J. K., Cotton, R., Marenco, F., Blyth, A., Cui, Z., Estelles, V., Gallagher, M., Coe, H., and Choularton, T. W.: Aircraft and ground measurements of dust aerosols over the west

African coast in summer 2015 during ICE-D and AER-D, Atmospheric Chemistry and Physics, 18, 3817-3838, 10.5194/acp-18-3817-2018, 2018b.

Mann, G. W., Carslaw, K. S., Spracklen, D. V., Ridley, D. A., Manktelow, P. T., Chipperfield, M. P., Pickering, S. J., and Johnson, C. E.: Description and evaluation of GLOMAP-mode: a modal global aerosol microphysics model for the UKCA composition-climate model, Geosci. Model Dev., 3, 519-551, 10.5194/gmd-3-519-2010, 2010.

McMeeking, G. R., Hamburger, T., Liu, D., Flynn, M., Morgan, W. T., Northway, M., Highwood, E. J., Krejci, R., Allan, J. D., Minikin, A., and Coe, H.: Black carbon measurements in the boundary layer over western and northern Europe, Atmospheric Chemistry and Physics, 10, 9393-9414, 10.5194/acp-10-9393-2010, 2010.

Moffet, R. C., and Prather, K. A.: In-situ measurements of the mixing state and optical properties of soot with implications for radiative forcing estimates, Proceedings of the National Academy of Sciences, 106, 11872-11877, 2009.

Motos, G., Schmale, J., Corbin, J. C., Zanatta, M., Baltensperger, U., and Gysel-Beer, M.: Droplet activation behaviour of atmospheric black carbon particles in fog as a function of their size and mixing state, Atmospheric Chemistry and Physics, 19, 2183-2207, 10.5194/acp-19-2183-2019, 2019.

Murphy, D. M., Cziczo, D. J., Froyd, K. D., Hudson, P. K., Matthew, B. M., Middlebrook, A. M., Peltier, R. E., Sullivan, A., Thomson, D. S., and Weber, R. J.: Single-particle mass spectrometry of tropospheric aerosol particles, Journal of Geophysical Research: Atmospheres, 111, n/a-n/a, 10.1029/2006jd007340, 2006.

Myhre, G., and Samset, B. H.: Standard climate models radiation codes underestimate black carbon radiative forcing, Atmospheric Chemistry and Physics, 15, 2883-2888, 10.5194/acp-15-2883-2015, 2015.

Olfert, J. S., and Collings, N.: New method for particle mass classification—the Couette centrifugal particle mass analyzer, Journal of Aerosol Science, 36, 1338-1352, 10.1016/j.jaerosci.2005.03.006, 2005.

Olfert, J. S., Reavell, K. S., Rushton, M. G., and Collings, N.: The experimental transfer function of the Couette centrifugal particle mass analyzer, Journal of Aerosol Science, 37, 1840-1852, 10.1016/j.jaerosci.2006.07.007, 2006.

Peng, J., Hu, M., Guo, S., Du, Z., Zheng, J., Shang, D., Levy Zamora, M., Zeng, L., Shao, M., Wu, Y.-S., Zheng, J., Wang, Y., Glen, C. R., Collins, D. R., Molina, M. J., and Zhang, R.: Markedly enhanced absorption and direct radiative forcing of black carbon under polluted urban environments, Proceedings of the National Academy of Sciences, 113, 4266-4271, 2016.

Péré, J. C., Mallet, M., Bessagnet, B., and Pont, V.: Evidence of the aerosol core-shell mixing state over Europe during the heat wave of summer 2003 by using CHIMERE simulations and AERONET inversions, Geophysical Research Letters, 36, 10.1029/2009gl037334, 2009.

Petzold, A., Ogren, J. A., Fiebig, M., Laj, P., Li, S. M., Baltensperger, U., Holzer-Popp, T., Kinne, S., Pappalardo, G., Sugimoto, N., Wehrli, C., Wiedensohler, A., and Zhang, X. Y.: Recommendations for reporting "black carbon" measurements, Atmospheric Chemistry and Physics, 13, 8365-8379, 10.5194/acp-13-8365-2013, 2013.

Ramanathan, V., and Carmichael, G.: Global and regional climate changes due to black carbon, Nature Geoscience, 1, 221, 10.1038/ngeo156, 2008.

Riemer, N., West, M., Zaveri, R. A., and Easter, R. C.: Simulating the evolution of soot mixing state with a particle-resolved aerosol model, Journal of Geophysical Research, 114, 10.1029/2008jd011073, 2009.

Riemer, N., and West, M.: Quantifying aerosol mixing state with entropy and diversity measures, Atmospheric Chemistry and Physics, 13, 11423-11439, 10.5194/acp-13-11423-2013, 2013.

Riemer, N., Ault, A. P., West, M., Craig, R. L., and Curtis, J. H.: Aerosol Mixing State: Measurements, Modeling, and Impacts, Reviews of Geophysics, 57, 187-249, 10.1029/2018RG000615, 2019.

Schroder, J. C., Hanna, S. J., Modini, R. L., Corrigan, A. L., Kreidenweis, S. M., Macdonald, A. M., Noone, K. J., Russell, L. M., Leaitch, W. R., and Bertram, A. K.: Size-resolved observations of refractory black carbon particles in cloud droplets at a marine boundary layer site, Atmospheric Chemistry and Physics, 15, 1367-1383, 10.5194/acp-15-1367-2015, 2015.

Schwarz, J. P., Spackman, J. R., Gao, R. S., Perring, A. E., Cross, E., Onasch, T. B., Ahern, A., Wrobel, W., Davidovits, P., Olfert, J., Dubey, M. K., Mazzoleni, C., and Fahey, D. W.: The Detection Efficiency of the Single Particle Soot Photometer, Aerosol Science and Technology, 44, 612-628, 10.1080/02786826.2010.481298, 2010.

Shannon, C. E.: A mathematical theory of communication, SIGMOBILE Mob. Comput. Commun. Rev., 5, 3-55, 10.1145/584091.584093, 2001.

Shi, Z., Vu, T., Kotthaus, S., Grimmond, S., Harrison, R. M., Yue, S., Zhu, T., Lee, J., Han, Y., Demuzere, M., Dunmore, R. E., Ren, L., Liu, D., Wang, Y., Wild, O., Allan, J., Barlow, J., Beddows, D., Bloss, W. J., Carruthers, D., Carslaw, D. C., Chatzidiakou, L., Crilley, L., Coe, H., Dai, T., Doherty, R., Duan, F., Fu, P., Ge, B., Ge, M., Guan, D., Hamilton, J. F., He, K., Heal, M., Heard, D., Hewitt, C. N., Hu, M., Ji, D., Jiang, X., Jones, R., Kalberer, M., Kelly, F. J., Kramer, L., Langford, B., Lin, C., Lewis, A. C., Li, J., Li, W., Liu, H., Loh, M., Lu, K., Mann, G., McFiggans, G., Miller, M., Mills, G., Monk, P., Nemitz, E., O'Connor, F., Ouyang, B., Palmer, P. I., Percival, C., Popoola, O., Reeves, C., Rickard, A. R., Shao, L., Shi, G., Spracklen, D., Stevenson, D., Sun, Y., Sun, Z., Tao, S., Tong, S., Wang, Q., Wang, W., Wang, X., Wang, Z., Whalley, L., Wu, X., Wu, Z., Xie, P., Yang, F., Zhang, Q., Zhang, Y., Zhang, Y., and Zheng, M.: Introduction to Special Issue – In-depth study of air pollution sources and processes within Beijing and its surrounding region (APHH-Beijing), Atmos. Chem. Phys. Discuss., 2018, 1-62, 10.5194/acp-2018-922, 2018.

Stephens, M., Turner, N., and Sandberg, J.: Particle identification by laser-induced incandescence in a solid-state laser cavity, Appl. Opt., 42, 3726-3736, 10.1364/AO.42.003726, 2003.

Sun, Y., Xu, W., Zhang, Q., Jiang, Q., Canonaco, F., Prévôt, A. S. H., Fu, P., Li, J., Jayne, J., Worsnop, D. R., and Wang, Z.: Source apportionment of organic aerosol from 2-year highly time-resolved measurements by an aerosol chemical speciation monitor in Beijing, China, Atmospheric Chemistry and Physics, 18, 8469-8489, 10.5194/acp-18-8469-2018, 2018.

Taylor, J. W., Allan, J. D., Allen, G., Coe, H., Williams, P. I., Flynn, M. J., Le Breton, M., Muller, J. B. A., Percival, C. J., Oram, D., Forster, G., Lee, J. D., Rickard, A. R., Parrington, M., and Palmer, P. I.: Size-dependent wet removal of black carbon in Canadian biomass burning plumes, Atmospheric Chemistry and Physics, 14, 13755-13771, 10.5194/acp-14-13755-2014, 2014.

Wang, J., Liu, D., Ge, X., Wu, Y., Shen, F., Chen, M., Zhao, J., Xie, C., Wang, Q., Xu, W., Zhang, J., Hu, J., Allan, J., Joshi, R., Fu, P., Coe, H., and Sun, Y.: Characterization of black carbon-containing fine particles in Beijing during wintertime, Atmospheric Chemistry and Physics, 19, 447-458, 10.5194/acp-19-447-2019, 2019.

Whittaker, R. H.: Vegetation of the Siskiyou Mountains, Oregon and California, Ecological Monographs, 30, 279-338, 10.2307/1943563, 1960.

Whittaker, R. H.: Dominance and Diversity in Land Plant Communities, Science, 147, 250-260, 1965.

Wu, Y., Wang, X., Tao, J., Huang, R., Tian, P., Cao, J., Zhang, L., Ho, K.-F., Han, Z., and Zhang, R.: Size distribution and source of black carbon aerosol in urban Beijing during winter haze episodes, Atmospheric Chemistry and Physics, 17, 7965-7975, 10.5194/acp-17-7965-2017, 2017.

Wu, Y., Cheng, T., Liu, D., Allan, J. D., Zheng, L., and Chen, H.: Light Absorption Enhancement of Black Carbon Aerosol Constrained by Particle Morphology, Environ Sci Technol, 10.1021/acs.est.8b00636, 2018.

Xie, C., Xu, W., Wang, J., Liu, D., Ge, X., Zhang, Q., Wang, Q., Du, W., Zhao, J., Zhou, W., Li, J., Fu, P., Wang, Z., Worsnop, D., and Sun, Y.: Light absorption enhancement of black carbon in urban Beijing in summer, Atmospheric Environment, 213, 499-504, 10.1016/j.atmosenv.2019.06.041, 2019.

Yang, J., McBride, J., Zhou, J., and Sun, Z.: The urban forest in Beijing and its role in air pollution reduction, Urban Forestry & Urban Greening, 3, 65-78, https://doi.org/10.1016/j.ufug.2004.09.001, 2005.

Zhang, X., Mao, M., Yin, Y., and Wang, B.: Numerical Investigation on Absorption Enhancement of Black Carbon Aerosols Partially Coated With Nonabsorbing Organics, Journal of Geophysical Research: Atmospheres, 123, 1297-1308, doi:10.1002/2017JD027833, 2018a.

Zhang, Y., Zhang, Q., Cheng, Y., Su, H., Li, H., Li, M., Zhang, X., Ding, A., and He, K.: Amplification of light absorption of black carbon associated with air pollution, Atmospheric Chemistry and Physics, 18, 9879-9896, 10.5194/acp-18-9879-2018, 2018b.
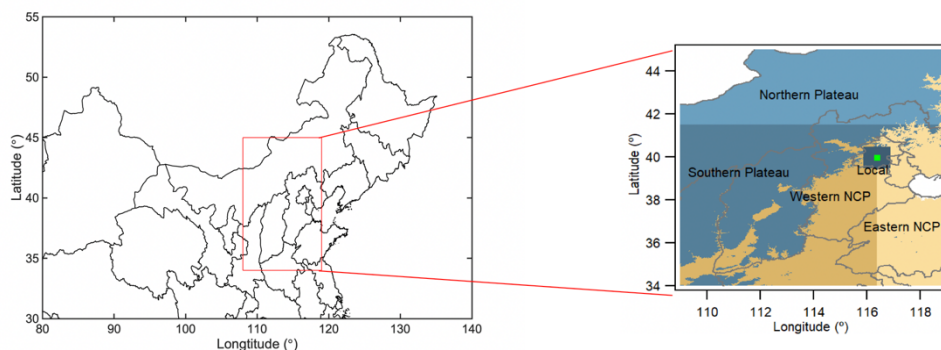
Figure 1 Classification of air mass sources (modified from Liu et al. (2018a))
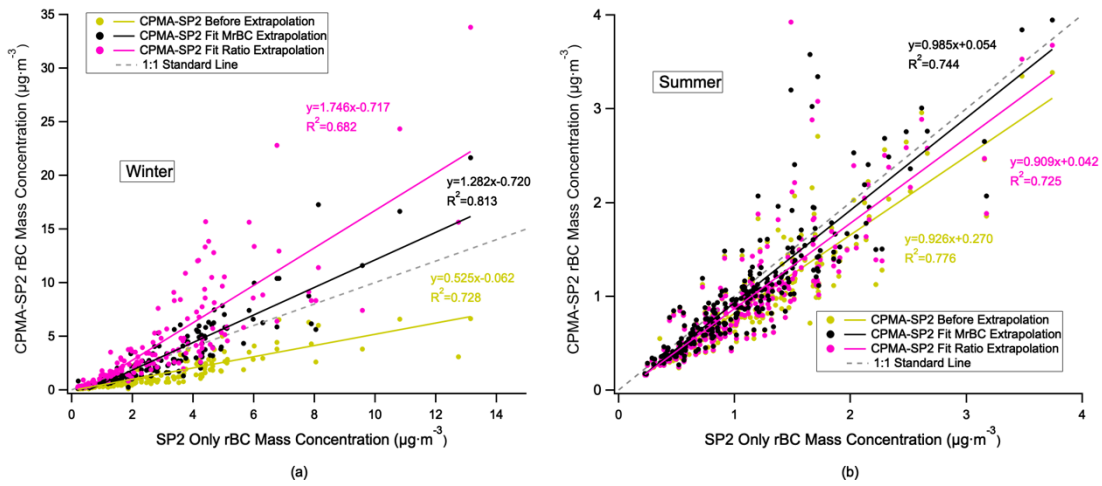
Figure 2 The rBC mass concentration comparison between SP2 only measurement and two different CPMA-SP2 extrapolation methods in winter (a) and summer (b)

(a)
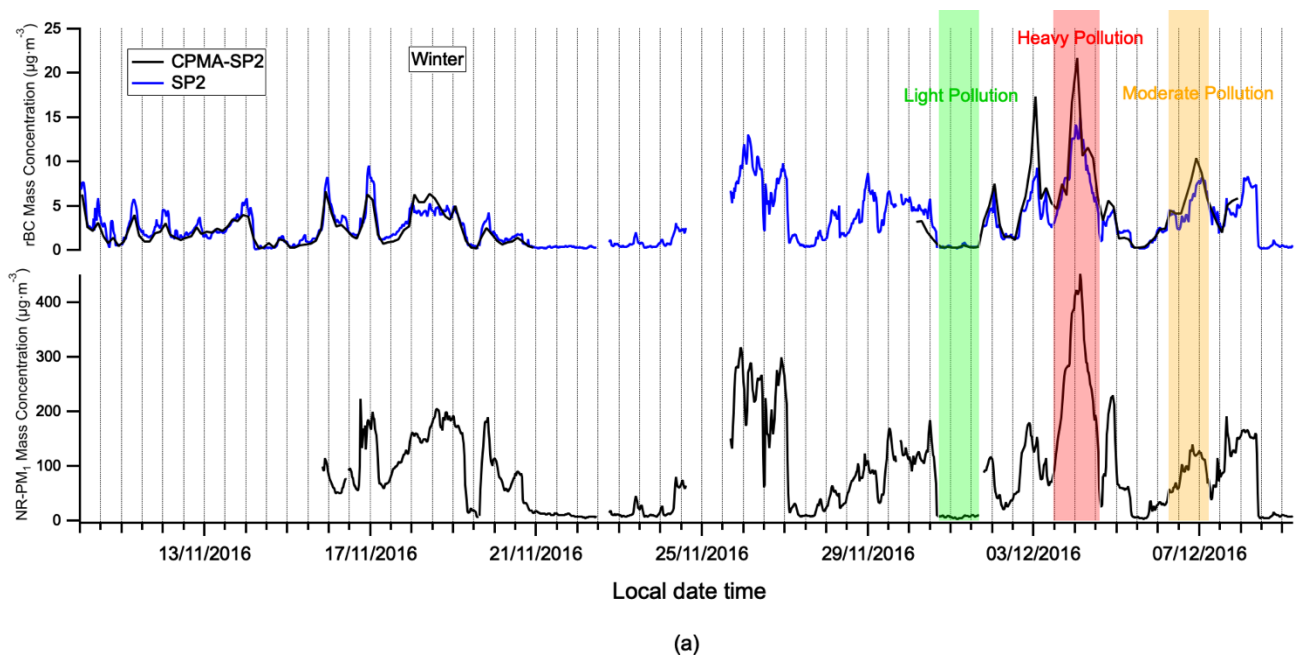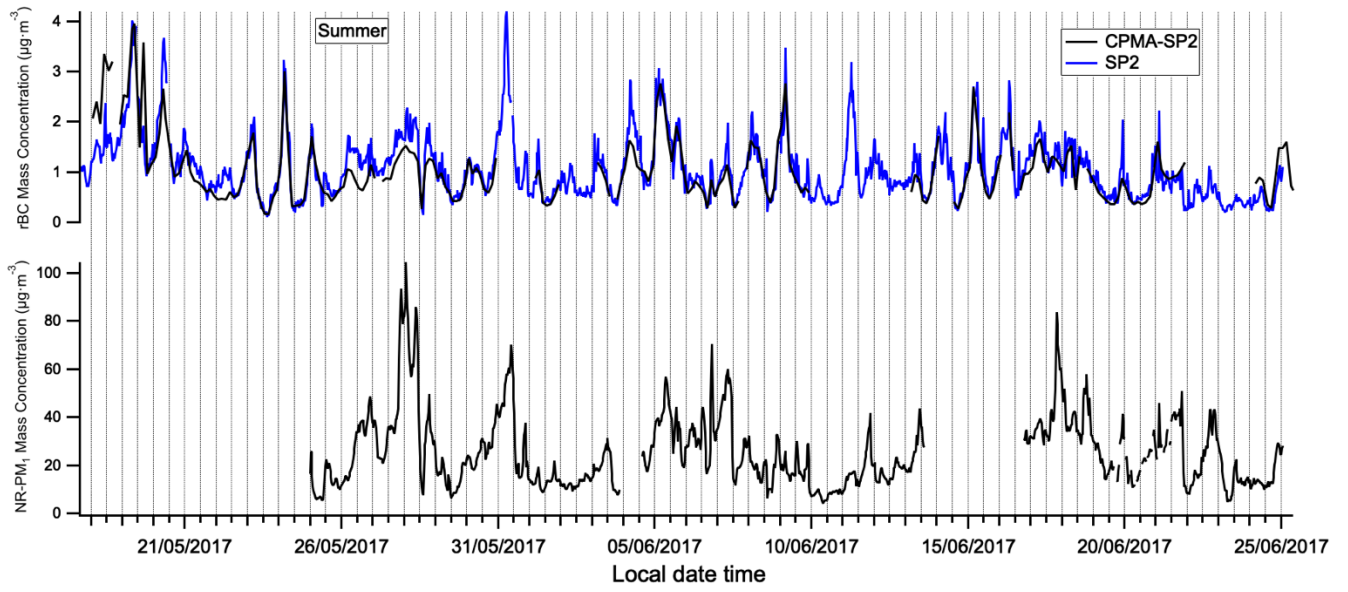
(b)

Figure 3 Time-series of rBC mass concentration and NR-PM$_1$ concentration for the winter (a) and summer (b) campaign
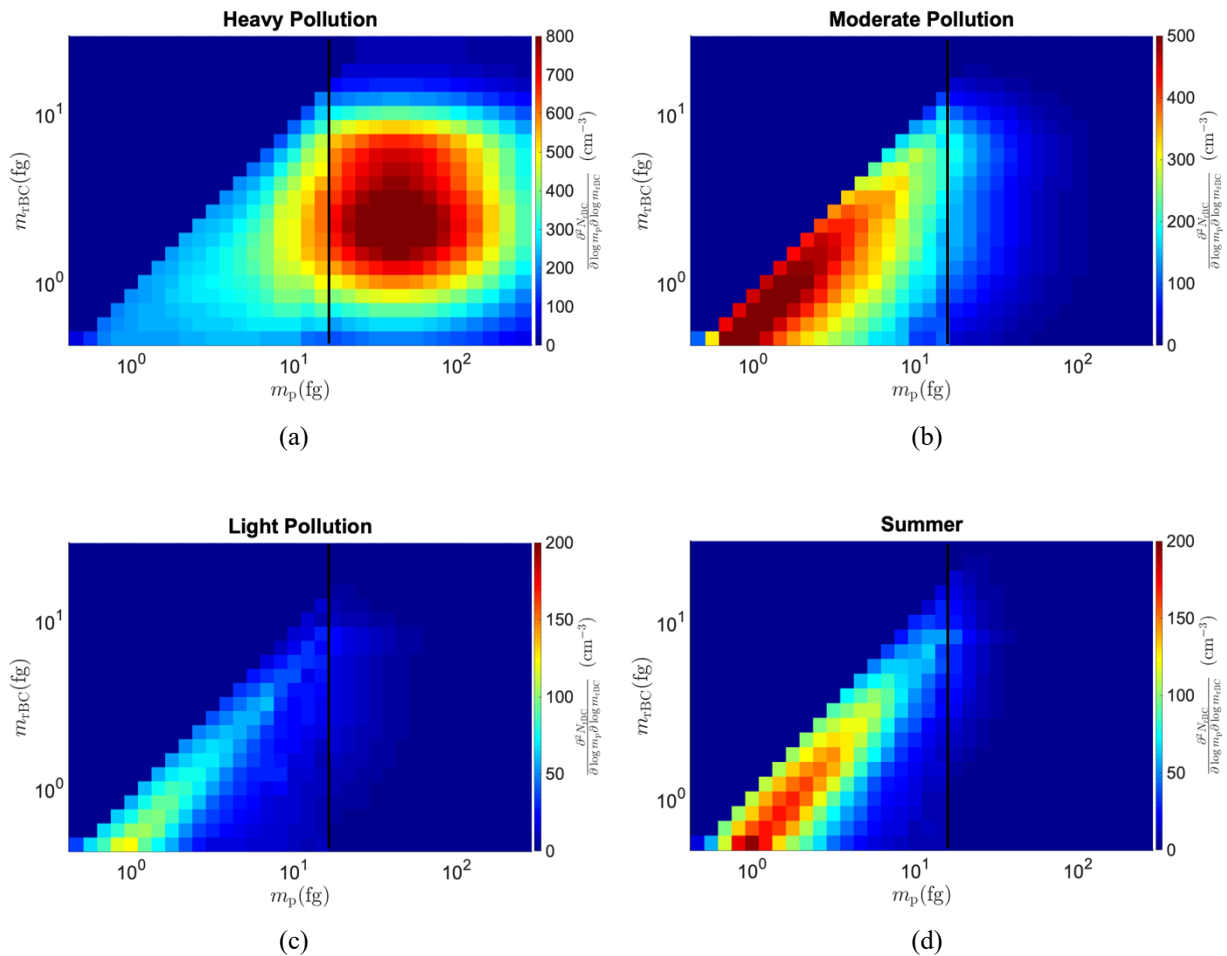
Figure 4 CPMA-SP2 Inversion matrix examples under different pollution conditions in winter (a, b, c), and the example in the summer period (d), the x-axis, m_p, represents the mass of the whole rBC-containing particle while the y-axis, m_rBC, represents the mass of the rBC material. The colour bar represents the magnitude of the two-variable distribution with a number concentration unit as cm^{-3}. All the bins with m_rBC larger than m_p are zero since such a particle does not exist in reality, and therefore the two-dimensional function distribution graph has a shape of triangle. The black solid line shows where the extrapolation starts.
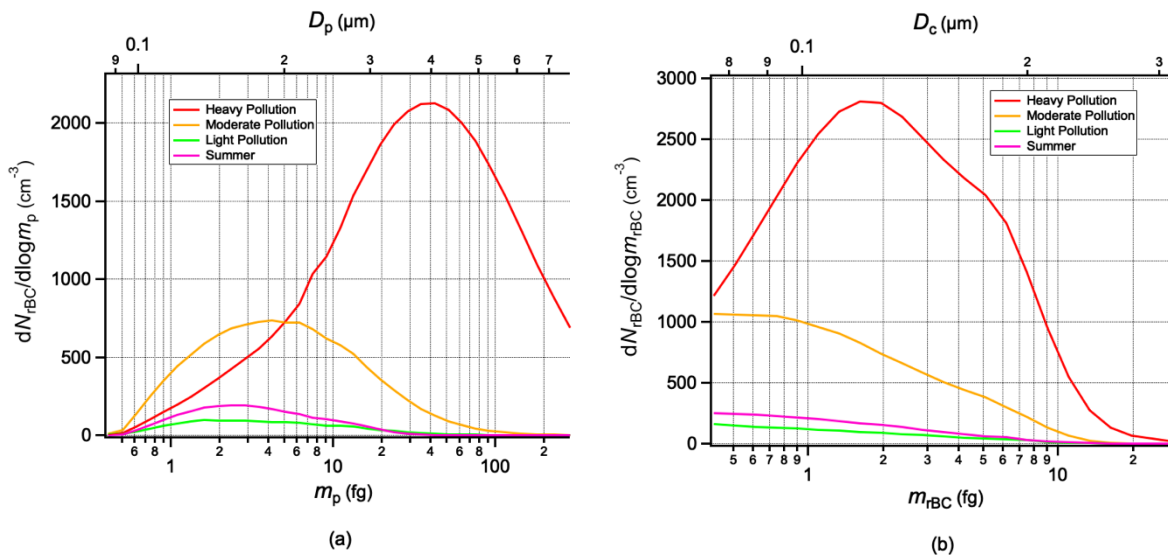
Figure 5 CPMA-SP2 m_p number distribution (a) and m_{rBC} number distribution (b) under different pollution conditions
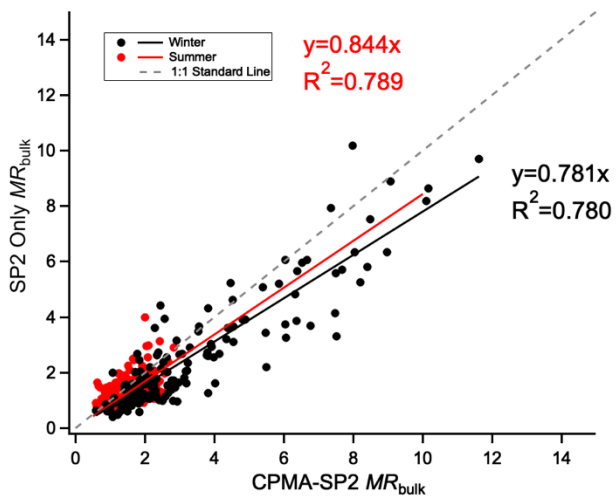
Figure 6 The comparison between bulk mass ratio (MR_{bulk}) from CPMA-SP2 method and from SP2 only method
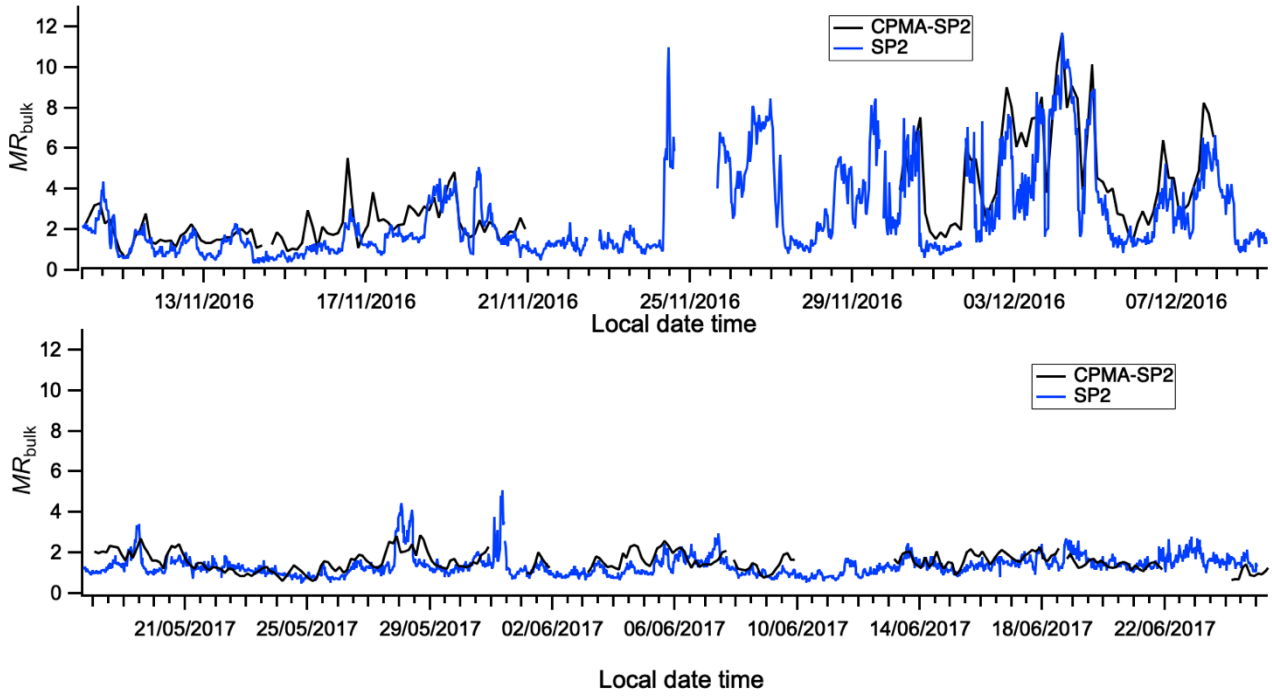
Figure 7 Time series of MR_{bulk} for winter and summer
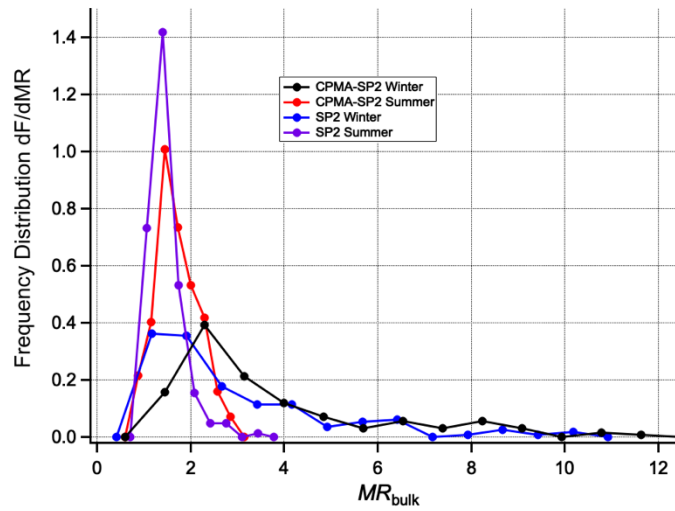
Figure 8 Frequency distribution of MR_{bulk} from both CPMA-SP2 and SP2 only method
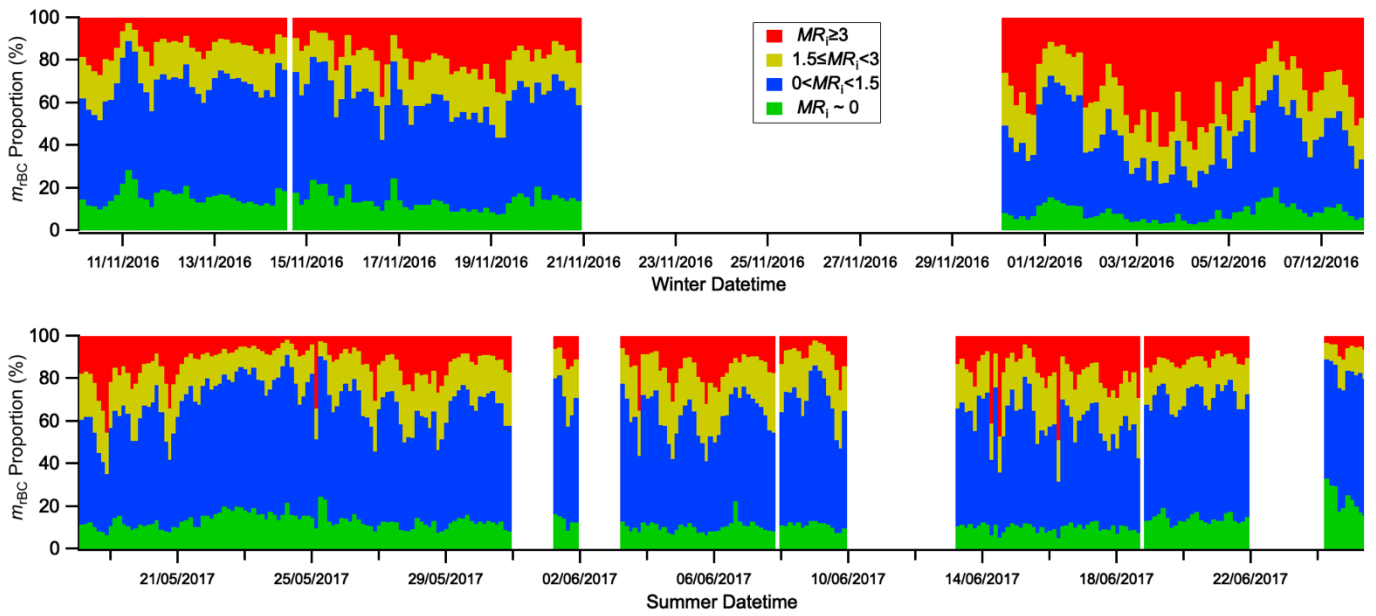
Figure 9 The evolution of rBC material mass fraction at different single particle MR (MR_i) level for winter and summer
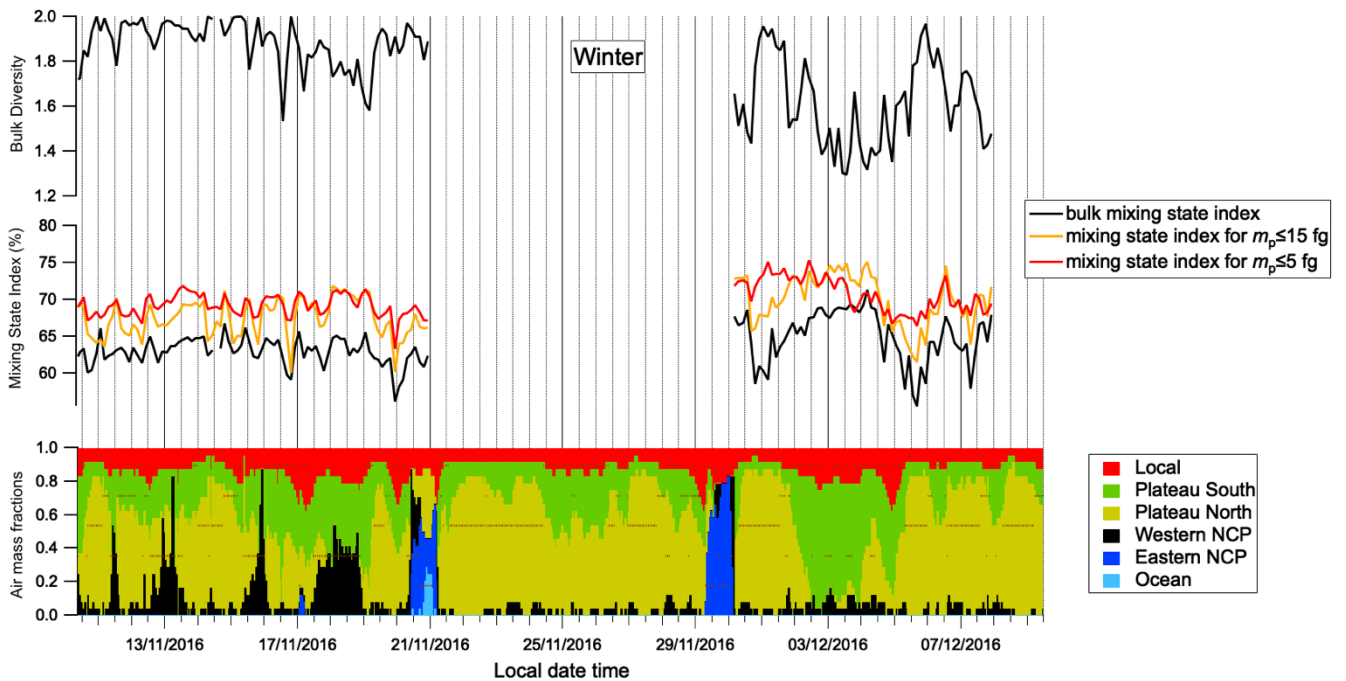
(a)
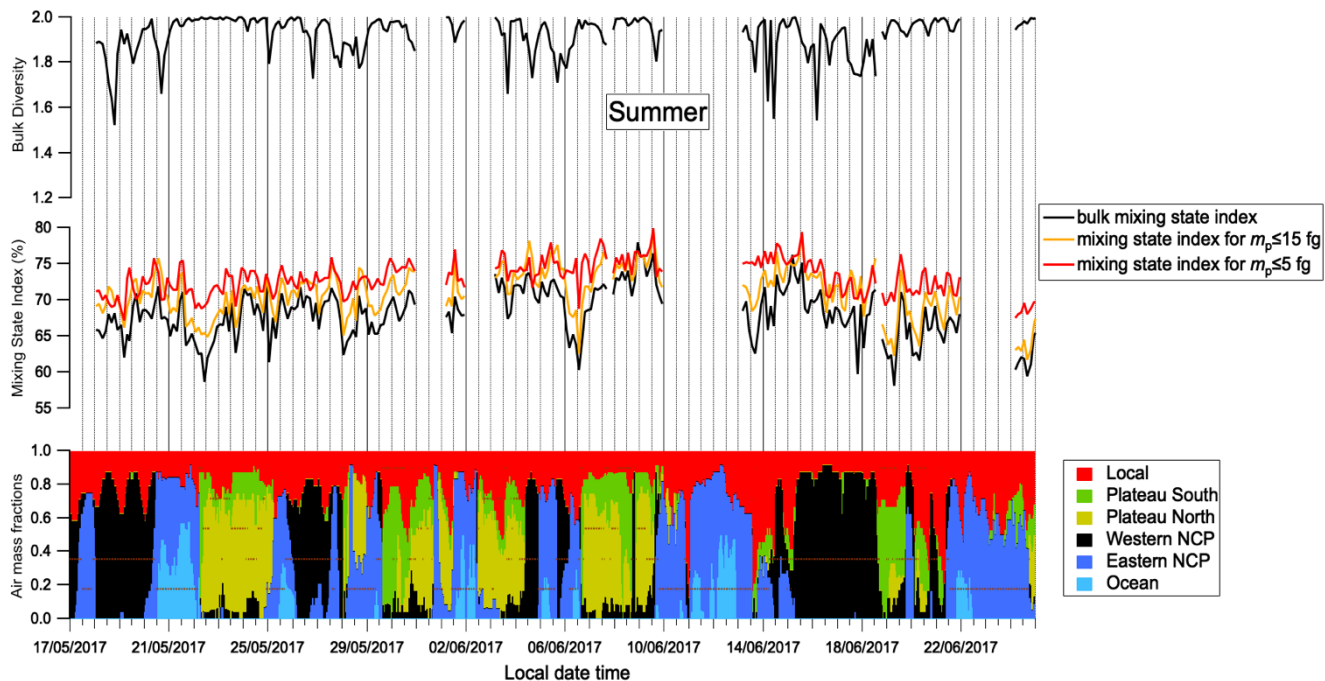
(b)

Figure 10 Bulk Diversity and Mixing State Index for the winter (a) and summer (b)
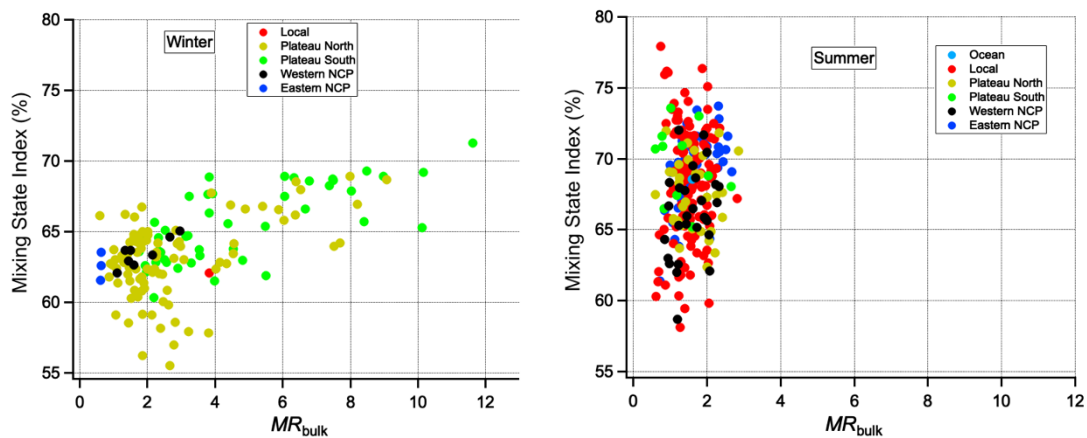
Figure 11 Air Mass Sources contribute to the MR and Mixing State Index for summer (a) and winter (b)
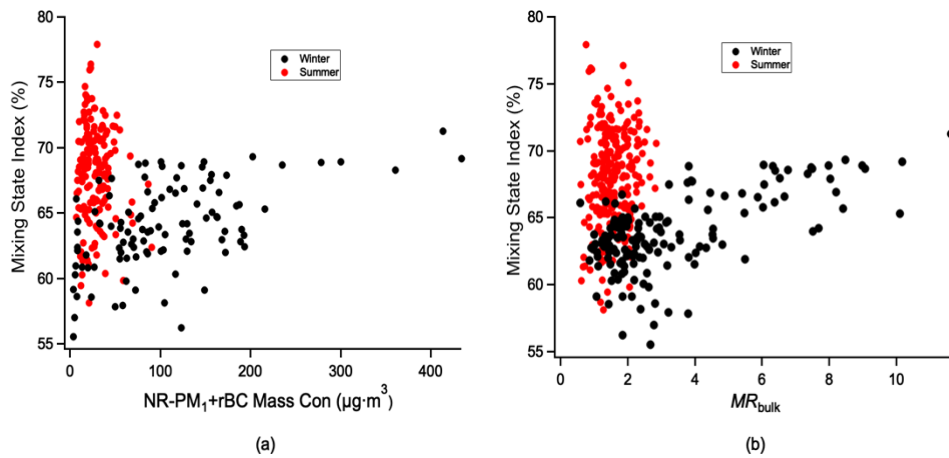
Figure 12 (a) The relationship between NR-PM$_1$ and rBC mass concentration and Mixing State Index, (b) the relationship between MR_{bulk} and Mixing State Index